Materials Today Bio 29 (2024) 101258

Contents lists available at ScienceDirect

Materials Today Bio

journal homepage: www.journals.elsevier.com/materials-today-bio

Injectable decellularized Wharton's jelly hydrogel containing CD56$^+$ umbilical cord mesenchymal stem cell-derived exosomes for meniscus tear healing and cartilage protection

Simiao Kang [a,1], Xin Shi [b,c,d,e,f,g,1], Yong Chen [b,c,d,e,f,g], Lin Zhang [b,c,d,e,f,g], Quanbo Liu [c,d,e,f,g], Ziyang Lin [b,c,d,e,f,g], Hongbin Lu [b,c,d,e,f,g,*], Haile Pan [a,**]

[a] Department of Sports Medicine and Joint Arthroplasty, Second Affiliated Hospital of Harbin Medical University, Harbin, 150086, China
[b] Department of Sports Medicine, Xiangya Hospital, Central South University, Changsha, 410008, China
[c] Key Laboratory of Organ Injury, Aging and Regenerative Medicine of Hunan Province, China
[d] Hunan Engineering Research Center of Sports and Health, Changsha, China
[e] Mobile Health Ministry of Education, China Mobile Joint Laboratory, Changsha, China
[f] Xiangya Hospital International Chinese Musculoskeletal Research Society Sports Medicine Research Centre, Changsha, China
[g] National Clinical Research Center for Geriatric Disorders, Xiangya Hospital, Central South University, Changsha, China

ARTICLE INFO

Keywords:
Meniscal tear
Decellularized Wharton's jelly hydrogel
CD56
Umbilical cord mesenchymal stem cell
Exosome

ABSTRACT

Traditional meniscectomy or suture for meniscal tear usually leads to failed self-healing, cartilage degeneration and worse osteoarthritis. The strategies that facilitate the healing process of torn meniscus and safeguard knee cartilage against degeneration will be promising for clinical therapy. The CD56$^+$ umbilical cord mesenchymal stem cells (UCSCs) (CD56$^+$UCSCs) were sorted from Wharton's jelly using flow cytometer. Then, the modified decellularized Wharton's Jelly hydrogel (DWJH) was combined with isolated CD56$^+$Exos from CD56$^+$UCSCs to fabricate DWJH/CD56$^+$Exos. The in vitro studies were performed to characterize the DWJ (decellularized Wharton's Jelly). The injectability and rheological properties were assessed by shear rate and frequency sweep analysis. The biocompatibility and chondrogenic differentiation inducibility of DWJH/CD56$^+$Exos were performed on human bone marrow mesenchymal stem cells (hBMSCs) and RAW 264.7 cells. The release dynamics was evaluated in vitro and in vivo experiments. As for the in vivo experiments, the operated rats that subjected to a 2 mm full-thickness longitudinal tear in right medial anterior meniscus were injected a single dose of DWJH/CD56$^+$Exos. At 4 and 8 weeks postoperatively, torn meniscus healing and articular cartilage degeneration were evaluated by hematoxylin and eosin (H&E), safranin O/fast green (SO&FG), and Sirius red staining. In in vitro experiments, the injectable DWJH/CD56$^+$Exos demonstrated excellent biocompatibility, exosome releasing efficiency, injectable property and chondrogenic inducibility. The results of in vivo experiments revealed that DWJH/CD56$^+$Exos degraded over time, promoted meniscal chondrogenesis, organized meniscal extracellular matrix remodeling, safeguard articular cartilage and inhibited secondary cartilage degeneration, which accelerated further facilitated torn meniscus healing. The novel injectable DWJH/CD56$^+$Exos promoted meniscal tear healing by promoting meniscal chondrogenesis, safeguarding articular cartilage, and inhibiting secondary cartilage degeneration.

* Corresponding author. Xiangya Hospital, No. 87, Xiangya Road, Kaifu District, Changsha, 410008, China
** Corresponding author. Department of Sports Medicine and Joint Arthroplasty, Second Affiliated Hospital of Harbin Medical University, No. 246 Baojian Road, Harbin, 150086, China.
E-mail addresses: hongbinlu@hotmail.com, hongbinlu@csu.edu.cn (H. Lu), panhaile_gzxz@hotmail.com (H. Pan).
[1] The two authors contributed equally to this paper.

https://doi.org/10.1016/j.mtbio.2024.101258
Received 4 July 2024; Received in revised form 2 September 2024; Accepted 17 September 2024
Available online 19 September 2024

1. Introduction

Meniscus plays a pivotal role in knee movement, including encompassing shock absorption and weight bearing [1]. With the increasing awareness of sports among individuals, meniscal injury caused by acute sports trauma or chronic degeneration has emerged as one of the most prevalent knee joint injuries [2,3]. Meniscal tears typically occur in avascular regions (white-white or red-white zone) and often fail to self-heal, resulting in altered stress distribution within the knee joint, secondary cartilage degeneration, and osteoarthritis [4,5]. The conventional clinical approach for treating meniscal tears involves partial or total excision and meniscal suture repair [6]. However, these methods only provide temporary pain relief for patients with a low success rate [7]. In the long run, an incomplete meniscus will accelerate cartilage degeneration and osteoarthritis progress. There were various treatments under investigation including exosomes, collagen matrix wrapping, bone marrow blood, factors, stem cells, as well as synthetic hydrogels et al. [3,8–12] However, these therapies exhibited certain limitations, including excessive degradation of exosomes and factors, insufficient biological activity of collagen or synthetic hydrogel, and immune reactions induced by cell transplantation [3,8–12]. Therefore, there is an urgent need for a treatment strategy that safeguards against articular cartilage degeneration and promotes torn meniscus repairing.

Exosomes are nanoscale vesicles secreted by cells and contain a diverse array of bioactive components [13]. Utilizing exosomes for biological therapy offers the advantage of circumventing immune and tumorigenic risks associated with cell transplantation [14]. Among the various sources of exosomes, umbilical cord mesenchymal stem cells (UCSCs) derived from medical waste, umbilical cords, are easily obtainable and widely applied in disease treatment [15,16]. However, due to the heterogeneity of stem cells, the therapeutic efficacy is limited in clinical trials [17,18]. The prevailing consensus suggested that exosomes derived from distinct subpopulations exhibited diverse biological functionalities [19]. Thus, standardizing these cells into specific functional subpopulations to achieve precise treatments could effectively facilitate their clinical translation applications. Currently, several surface biomarkers had been developed that enabled characterization and screening of cell subpopulations with significant biological functions. Relevant studies had demonstrated that $CD56^+$ cells within mesenchymal stem cell play a role in cartilage regeneration [20]. Furthermore, single-cell RNA sequencing analysis had provided insights into the expression patterns of CD56 within chondroblast subpopulation [21]. Therefore, the application of $CD56^+$ mesenchymal stem cell (MSC) derived exosomes may offer a promising avenue for enhancing cartilage regeneration. However, direct utilization of exosomes was hindered by their rapid clearance and degradation within the environment of injured knee [22–24]. Thus, devising strategies to safeguard exosomes and facilitate their sustained release represents an effective solution.

The Wharton's jelly derived from the umbilical cord is abundant in collagen, proteoglycan, and other nutrient factors, which exhibits lubricating, protective, and nourishing effects for the knee joint cartilage [25–27]. However, Wharton's jelly containing cellular components may potentially elicit immune reactions and promote tumor formation [25]. Additionally, the solid Wharton's jelly for the treatment of meniscal tears presents inherent challenges [28]. To address these concerns, decellularized Wharton's jelly hydrogel (DWJH) could be an excellent choice by removing cellular components meanwhile preserving the extracellular matrix. Furthermore, the combination of DWJH and exosomes (named DWJH/$CD56^+$Exos) enabled sustained release of exosomes, which enhancd therapeutic efficacy and reduced treatment cost.

CD56, also known as neural cell adhesion molecule (NCAM), is a surface marker that has been used to identify a subpopulation of MSCs with enhanced chondrogenic potential. Battula et al. discovered that effective chondrocyte differentiation could only be induced in human $CD56^+$ BMSCs, wheras adipocytes were exclusively derived from $CD56^-$ BMSCs in vitro [20]. Wang et al. demonstrated the chondrogenic potential of $CD56^+$ chondrocyte precursors within the subpopulation of bone marrow-derived mesenchymal stem cells (BMSCs) through comprehensive internal and external experiments combining single-cell RNA sequencing [21]. However, limited research had been conducted on $CD56^+$ stem cells derived from Wharton's jelly. We applied decellularized technology to modify the physical properties and eliminate cellular components of the Wharton's jelly, meanwhile preserving the extracellular matrix that could safeguard cartilage against degeneration. In this study, we isolated exosomes from $CD56^+$UCSCs obtained through flow cytometry from Wharton's jelly. The $CD56^+$ exosomes were integrated with injectable decellularized Wharton's jelly hydrogel for meniscal tear in rat. In vitro experiments confirmed that DWJH/$CD56^+$Exos exhibited excellent biocompatibility and promoted chondrogenic differentiation in human bone marrow mesenchymal stem cells (hBMSC) as well as migration and proliferation. Subsequently, in vivo experiments further validated the reparative effects of DWJH/$CD56^+$Exos for meniscus tear in rat and its protective effects against knee cartilage degeneration. In conclusion, our developed injectable DWJH/$CD56^+$Exos demonstrated potential for promoting meniscus tear repairing and providing cartilage protection. DWJH/$CD56^+$Exos offered a minimally invasive treatment option for clinic treatment.

2. Materials and methods

The animal experiment was conducted in accordance with the National Institutes of Health guide for the care and use of laboratory animals (NIH Publications No. 8023, revised 1978). Male Sprague-Dawley (SD) rats weighing between 250 and 350g were obtained from the Experimental Animal Center of Central South University to establish the meniscus tear model and perform in vivo degradation assay. The experimental procedures were performed following ethical approval from the Ethics Committee of Xiangya Hospital, Central South University (CSU-2024-0038). Ethical certification was obtained from Xiangya Hospital, Central South University for sourcing umbilical cords used in $CD56^+$UCSCs preparation and DWJH.

2.1. $CD56^+$ UCSCs isolation

The collected umbilical cords were washed three times with phosphate-buffered saline (PBS) containing 1 % penicillin-streptomycin (P/S). Under sterile conditions, the outer amnion and the arteries and veins were excised. The collected Wharton's jelly was minced into chylous shape, followed by addition of 3 ‰ hyaluronidase and 3 ‰ type II collagenase. The mixture was then incubated in a constant temperature shaking bed at 37 °C for 1 h. Subsequently, the suspension was filtered and centrifuged to obtain cell precipitate, half of which was directly seeded in a T25 culture flask and cultured in an incubator with 5 % CO_2 at 37 °C. The remaining half of the cells were treated with Human BD Fc Block solution (564219, BD, USA) at 4 °C for 10 min. Then, Zombie Aqua (423101, Biolegend, USA) was added to the cell suspension and incubated at room temperature for 15 min, followed by addition of specific antibodies at 4 °C for 30 min: anti-CD235a-PE (61-9987-42, eBioscience™, USA), anti-CD31-BB515 (564430, BD, USA), anti-CD45-PerCP-Cyanine5.5 (45-0459-42, eBioscience™, USA), anti-CD73-BV421(562430, BD, USA), and anti-CD56-PE/Cyanine7 (318318, Biolegend, USA). After washing off excess antibodies, the cells were resuspended in FACS buffer. $CD56^+$UCSCs were isolated using FlowJo software(BD,USA)and expanded to P3 generation for subsequent experiments.

2.2. Identification of $CD56^+$UCSCs

To identify $CD56^+$UCSCs, the P3 generation cells were enzymatically digested with 0.25 % pancreatic enzymes when they reached 70–80 % confluence. For three-lineage differentiation, the cells were seeded in

12-well plates at a density of 2×10^4 cells/cm^2. The corresponding culture medium for osteogenesis, chondrogenesis, and lipogenesis differentiation was added according to the provided instructions (Haixing Biotechnology, China). Following incubation for a specified duration, Alizarin red, oil red O, and Alcian blue staining were employed to detect osteogenic, chondrogenic, and adipogenic differentiation of CD56$^+$UCSCs. Flow cytometry analysis was performed using antibodies against CD11b-PE/Cyanine5 (301308, Biolegend, USA), CD34-APC/Cyanine7 (343514, Biolegend, USA), CD45-PerCP-Cyanine5.5 (45-0459-42, eBioscience™, USA), CD29-PE (303004, Biolegend, USA), CD73-BV421(562430, BD, USA), and CD56-PE/Cyanine7 (318318, Biolegend, USA).

2.3. Isolation and evaluation of exosomes derived from CD56$^+$UCSCs

When UCSCs or CD56$^+$UCSCs reached 70–80 % confluence for isolation of exosomes, the culture medium was aspirated and washed with PBS. Subsequently, complete medium containing 10 % non-exosome serum was added. The cells were then cultured at 37 °C with 5 % CO_2 for 48 h. Afterwards, the collected supernatant was clarified to remove cell debris and filtered using a 0.22 μm filter. Following the manufacturer's instructions, the filtered supernatant was mixed with Exoquick-TC Exosome Precipitation Solution (SBI, USA) at 4 °C overnight for incubation. Exosomes were subsequently isolated from the mixture by centrifugation at 120,000 g for 1 h and cryopreserved in PBS at −80 °C for subsequent experiments. Transmission electron microscopy (TEM; FEI, USA) and nanoparticle tracking analysis (NTA) assays were employed to characterize the physical properties of isolated exosomes. Additionally, western blot (WB) was performed to detect exosome markers including TSG101 (28283-1-AP, proteintech, USA), CD63 (25682-1-AP, proteintech, USA), and CD81 (66866-1-AP, proteintech, USA).

To evaluate the cellular uptake of exosomes by hBMSCs, the hBMSCs were incubated with PKH26-labeled exosomes. Briefly, UCSC-Exos or CD56$^+$UCSC-Exos were incubated with PKH26 staining solution according to the instruction of PKH26 red fluorescent cell membrane staining kit (D0030, Solarbio, China). Then, the mixture was mixed with Exoquick-TC Exosome Precipitation Solution (SBI, USA) to isolate the PKH26-labeled exosomes, which was consistent with the above exosome extraction method. Subsequently, the hBMSCs were incubated with PKH26-labeled exosomes (50 μg/ml) for 12 h at 37 °C, protected from light. After PBS washing, the cells were fixed in 4 % paraformaldehyde for 15 min and rinsed thrice with PBS. Subsequently, the fixed cells were incubated with phalloidin at room temperature under light protection for 30 min. Excess dye was removed by washing thrice with PBS, each time lasting for 5 min. Finally, cellular uptake of exosomes was visualized using a fluorescence microscope (Zeiss, Solms, Germany) after staining the cell nuclei with DAPI (Invitrogen, Carlsbad, USA).

The chemotactic ability of CD56$^+$UCSC-Exos was evaluated using a transwell assay. In the lower chamber, 600 μl medium containing UCSC-Exos or CD56$^+$UCSC-Exos (50 μg/ml) was added and the plate without exosomes served as a control group. The hBMSCs (1×10^4) were seeded in the upper chamber and incubated at 37 °C for 24 h. Subsequently, the chambers were washed with PBS and fixed with formaldehyde. Migrated cells were stained with a solution of 0.5 % crystal violet, which shown purple appearance under an optical microscope.

The chondrogenic inducibility of UCSC-Exos or CD56$^+$UCSC-Exos on hBMSC differentiation was evaluated by co-culturing with hBMSC. Briefly, hBMSCs were co-cultured with either UCSC-Exos or CD56$^+$UCSC-Exos, while the culture plate served as the control group. After 14 days (at a density of 1.5×10^7/mL), the co-cultured cells were stained using Alcian blue staining to detect chondrogenic differentiation. Following a 14-day co-culture period (at a density of 2×10^5/cm^2), the plates were washed thrice with PBS and fixed using 4 % paraformaldehyde. Subsequently, cell membranes were permeabilized using 0.1 % Triton X-100 (Sigma-Aldrich) and nonspecific binding was blocked by applying 3 % bovine serum albumin. Primary antibodies against SOX9 (ab185966; Abcam) were then added, followed by incubation with corresponding secondary antibodies. Confocal microscopy (TCS-SP8; Leica) was utilized for image acquisition and quantification of positive cells. Additionally, RNA extraction was performed, and quantitative real-time polymerase chain reaction (qRT-PCR) assay was conducted to analyze SOX9, COL10, and ANCA expression in the co-cultured cells. The primer sequences are provided in Table 1.

2.4. Preparation of DWJ

To obtain decellularized Wharton's jelly (DWJ), the collected umbilical cord was rinsed thrice in sterile PBS. Subsequently, the umbilical cord was cut into 5 cm length and longitudinally dissected after removing the amniotic membrane. The arterio-vein of the umbilical cord was excised. Then, the Wharton's jelly was minced into particles measuring 1 mm^3. These particles were then incubated at 4 °C in a solution containing 10 mM Tris buffer and 5 mM ethylenediaminetetraacetic acid (EDTA) in water for 10 h. After that, the solution was replaced with a mixture of pure water containing 1 % Triton X-100, 1 M potassium chloride (KCl), and 50 mM Tris buffer, followed by incubation on a shaker at 4 °C for 12 h. Afterwards, the samples were washed thrice with sterile PBS for 1 h each time. The washed samples were then immersed in sterile normal saline supplemented with RNase (100 μg/ml) and DNase (150 IU/ml) (S8820-20TAB, Sigma, USA)), followed by incubation on a constant temperature shaking bed at 37 °C for 6 h. Decellularized Wharton's jelly particles were obtained by soaking the nuclease-digested sample with sterile PBS thrice for 1 h each time before being frozen at −80 °C for further use.

2.5. Evaluation of DWJ

To evaluate the condition of Wharton's jelly before and after decellularization, decellularized and native samples were fixed in 4 % (vol/vol) paraformaldehyde for 24 h. Subsequently, the samples underwent dehydration, embedding, and sectioning into 5 μm slices for assessment of residual nuclear fragments and retention of extracellular matrix (ECM) using hematoxylin and eosin (H&E) and 4′,6-diamidino-2-phenylindole (DAPI). Besides, the residual DNA content from DWJ was extracted and quantified using PicoGreen dsDNA assay kit (Invitrogen, USA). For microstructural analysis of decellularized samples, fixation with 2.5 % glutaraldehyde was followed by lyophilization, gold spraying, and examination via scanning electron microscopy (SEM). Additionally, to quantitatively determine proteoglycan and collagen content within decellularized Wharton's jelly samples following previously established methods [29,30], sections were subjected to a synchrotron radiation Fourier transform infrared spectroscopy (SR-FTIR) at the BL01B beamline located at the National Facility for Protein Science Shanghai (Shanghai Synchrotron Radiation Facility, China). The distribution and content of collagen and proteoglycan were characterized by calculating the peak areas corresponding to amide I (1720-1590 cm^{-1}) and carbohydrate regions (1140-985 cm^{-1}), respectively [29,31].

To quantify the content of the proteoglycan and collagen in DWJ and native Wharton's jelly, the acquired particles were lyophilized. Then the lyophilized particles were applied to detect the content of proteoglycan

Table 1
Primer sequences.

Genes	Primers and probe sequences	
ACAN	F	5′-CTATACCCCAGTGGGCACAT-3′
	R	5′-GGCACTTCAGTTGCAGAAGG-3′
SOX-9	F	5′-GCCGACCAGTACCCGCACCT-3′
	R	5′-CGCCTGCCCATTCTTCACCGACT-3′
COL10	F	5′-CACGTTTGGGTAGGCCTGTA-3′
	R	5′-TCTGTGAGCTCCATGATTGC-3′

and collagen in accordance with the instructions provided in Glycosaminoglycan Assay Kit (NJJC-H480-1, China) and Soluble Collagen Assay Kit (CBL-MET-5016, Cell Biolabs, USA), respectively.

2.6. Preparation of DWJH/CD56$^+$Exos

To prepare the injectable decellularized Wharton's jelly hydrogel (DWJH), the freeze-dried and finely ground decellularized Wharton's jelly granules were subjected to extracellular matrix (ECM) extraction using the published urea dissolution method [32,33]. The granules were mixed with a 3 M urea solution at a ratio of 1:10 (w/v) and stirred at 4 °C for 2 days. After centrifugation of the mixture at 2000g for 15 min, the supernatant was dialyzed using a benzoylated dialysis tube (Sigma-Aldrich) in ultra-pure water for 24 h, meanwhile the ultra-pure water was changed every 6 h. The purified ECM solution was enriched via centrifugation in an ultrafiltration tube (2000 MWCO, Sigma-Aldrich, USA) at 2000g for 30 min before being sterilized through a 0.22 μm filter. The filtered solution was injectable DWJH. The protein concentration of DWJH was subsequently determined using the BCA detection kit (E-BC-K318-M, Elabscience, China) and frozen at a concentration of 1 mg/mL, followed by storage at −80 °C for future use. The DWJH/CD56$^+$Exo or DWJH/Exo composite was formulated by homogenously blending CD56+Exo or Exo with DWJH at a weight-to-volume ratio of 1:100.

2.7. Characteristics and biocompatibility of DWJH/CD56$^+$Exos

The prepared hydrogel underwent freeze-drying and gold-spraying procedures before being characterized for microstructural analysis using SEM. The hydrogel sample was loaded into a 1 mL syringe to evaluate its injectability, while different shapes were formed by injecting the hydrogel manually. The rheology measurement of DWJH/CD56$^+$Exos was detected by scientific-grade rheometer (Malvern Kinexus pro+, British). The exposed surface of the sample was coated with a thin layer of silicone oil to prevent water evaporation during the experiments, and all measurements were conducted at a temperature of 37 °C. The shear rate was incrementally increased from 10^{-2} to 10^3 s^{-1} in a stepwise manner. Frequency sweep analysis was conducted across an angular frequency (ω) range of 100-0.1 rad s^{-1}, with an initial strain (γ) of 1 %.

To evaluate cellular viability within the context of DWJH/CD56$^+$Exo treatment, hBMSCs were co-cultured at a density of 2×10^5/cm^2 along with this composite material, while an empty culture plate served as control. Following a period of 72 h post-co-culture incubation, Yeasen's CALCIN-AM/PI double staining kit (40747ES76) was utilized for labeling these co-cultivated cells. Subsequently, fluorescent microscopy employing Zleica equipment (with excitation wavelengths set at either 488 nm or 594 nm) enabled visualization and determination regarding any influence exerted by DWJH/CD56$^+$Exo formulation upon cellular survival rates - green indicating viable cells whereas red denoting deceased ones. Additionally, on days 1, 3, 5,7 and 9 post-co-culture, Cell Counting Kit-8 (CCK-8) assay was utilized to evaluate effect pertaining to DWJH/CD56$^+$Exo-induced cell prolife. The absorbance of the co-culture system was measured at specified time points using a Thermo Scientific microplate reader, with an optical density of 450 nm, after treatment with CCK-8 reagent. The RAW 264.7 cells (5.0×10^4 cells/well) (Pricella) were co-cultured with DWJH/CD56$^+$Exo to evaluate the proinflammatory properties of DWJH/CD56$^+$Exo. The experimental groups included a negative control group treated with complete medium only (Control group), a proinflammatory control group supplemented with 10 μg/mL lipopolysaccharide (Sigma-Aldrich, USA) (LPS group), and a group treated with complete medium containing DWJH/CD56$^+$Exo (DWJH/CD56$^+$Exo group). On day 3, cell protrusions were observed to examine the morphology of RAW 264.7 cells, and ELISA kits (Elabscience, China) were employed to quantify the levels of TNF-α, IL-6, and IL-1β in the culture supernatant.

2.8. Chondrogenesis of hBMSC induced by DWJH/CD56$^+$Exos

To assess the chondrogenic differentiation potential of DWJH/CD56$^+$Exos in hBMSC, hBMSCs were co-cultured with CD56$^+$Exos, DWJH or DWJH/CD56$^+$Exos, while culture plate was used as the control group. Following 14 days (at a density of 1.5×10^7/mL) of co-culture, chondrogenic differentiation was evaluated by Alcian blue staining. After 14 days of co-culture (at a density of 2×10^5/cm^2), cells were washed three times with PBS and fixed with 4 % paraformaldehyde. Subsequently, cell membrane permeabilization was achieved using 0.1 % Triton X-100 (Sigma-Aldrich), followed by blocking non-specific binding using 3 % bovine serum albumin. The cells were then incubated with anti-SOX9 antibody (ab185966; Abcam) and corresponding secondary antibody for detection. Confocal microscopy (TCS-SP8; Leica) was used for image acquisition and positive cell quantification. The proteins obtained from co-cultivated cells underwent RIPA treatment (Solarbio, China) followed by quantification using a BCA kit. Subsequently, these proteins were separated through 10 % SDS-PAGE and transferred onto PVDF membranes via electrophoresis. Blocking of the membranes was performed using 5 % fat-free milk before overnight incubation with primary antibodies including anti-SOX9 (ab185966, abcam, USA), anti-COL2 (28459-1-AP, proteintech, USA), anti-COLX (DF13214, affinity, USA), and anti-GAPDH (10494-1-AP, Proteintech, USA). After thorough washing steps had been carried out, the corresponding HRP-labeled secondary antibodies (E-AB-1003, Elabscience, China) were applied to the membranes for a duration of 90 min at room temperature. Subsequently, the immune response bands on the membrane surface were detected using enhanced chemiluminescence reagents (New Cell & Molecular Biotech, China).

2.9. Sustained release of CD56$^+$Exos from DWJH/CD56$^+$Exos

The sustained release of CD56$^+$Exos from DWJH/CD56$^+$Exos was evaluated both in vivo and in vitro. For the in vitro release study, CD56$^+$Exos labeled with PKH26 were placed onto a plate supplemented with PBS and incubated at 37 °C with 5 % CO_2. The PBS solution was replaced every 24 h. At 0, 7, 14, and 21 days, the incubated DWJH/CD56$^+$Exos samples were observed under a fluorescence microscope and subjected to three-dimensional reconstruction analysis. For the release kinetics of CD56$^+$Exos from DWJH/CD56$^+$Exos, 100 μL hydrogel was loaded into the upper chamber of a 24-well plate, while 500 μL PBS was added to the lower chamber and maintained at 37 °C. At regular intervals, an equivalent volume of fresh PBS medium was replenished after collecting 500 μL of each sample. The quantitative determination of exosome release was performed using the Micro BCATM Protein Assay Kit (ThermoFisher, USA). The release profile was plotted based on these measurements. In the case of in vivo DiR-labeled CD56$^+$Exos release assessment, post-operative rats were injected with equal amounts of DWJH/CD56$^+$Exos or saline + CD56$^+$Exos. The intensity and distribution of DiR signals were detected using a non-invasive tracking system (IVIS Spectrum, PerkinElmer, United States).

2.10. In vivo degradation

The in vivo injectability and degradation of the DWJH/CD56$^+$Exos was assessed in a rat subcutaneous model [34]. To check injectability and degradation in vivo, 100 μL hydrogel was subcutaneously injected into rat dorsal regions via a 26-gauge needle. After 30 min, the injected sites were excised to check the hydrogel formation. For in vivo biocompatibility evaluation, the hydrogel with surrounding tissues were excised at days 3, 7, 14, and 21 after implantation. The collected samples were embedded in OCT and sectioned into 7 μm thick slices for H&E staining. Then, the stained slices were photographed under microscope.

2.11. Meniscus tear model and injection of DWJH/CD56$^+$Exos

The meniscus tear model was performed as previously described [35,36]. Briefly, preoperative prophylaxis was administered through intramuscular injection of penicillin (100,000 U/kg). Then, SD rats were anesthetized by intraperitoneal injection of pentobarbital sodium (40 mg/kg) dissolved in saline solution. Subsequently, the right knee was exposed using the medial parapatellar approach with lateral patella dislocation, allowing for identification of the avascular zone (white--white zone) of the medial meniscus at full flexion. A 2 mm full-thickness longitudinal tear was then created in this region using a scalpel. Following suturing of the joint capsule and skin sequentially, rats received a 30 μL intra-articular injection of either saline, DWJH or DWJH/CD56$^+$Exos using an insulin syringe. After surgery, rats were returned to their cages and allowed unrestricted movement and access to food. The rats were euthanized at 4 and 8 weeks, followed by excision of the operative meniscus, femoral condyle, and tibial plateau from the right knee joint for subsequent testing.

2.12. Histological evaluation of femoral condyle and tibial plateau

To evaluate the degeneration of articular cartilage, the femoral condyle and tibial plateau on the operative side were isolated and fixed in a 4 % (vol/vol) paraformaldehyde solution. Subsequently, decalcification was performed using 0.5 M EDTA fluid. After dehydration through an increasing alcohol gradient, the decalcified specimens were embedded in paraffin and sectioned into 5-μm slides in both coronal plane at the midpoint of the tibial plateau and sagittal plane at the midpoint of the medial femoral condyle [37]. These slides underwent H&E staining as well as safranin O/fast green staining for assessment of articular cartilage degradation. The International Cartilage Regeneration & Joint Preservation Society (ICRS) grading system along with Mankin grading system were independently employed by three colleagues to blind assess this degradation [38].

2.13. Histological evaluation of meniscus

Following the excision of excessive tissue, the harvested meniscus was fixed in 4 % neutral paraformaldehyde. Subsequently, the fixed meniscus underwent decalcification, dehydration, and embedding in paraffin. Then the embedded samples were sectioned into 5 μm slices for H&E staining, safranin O/fast green staining, and Sirius red staining. The healing process of the meniscus was assessed by calculating the ratio of torn area in different groups to that in the control group at each time point.

2.14. Statistical analysis

The statistical analysis included one-way ANOVA and the Student t-test to determine if there were any significant differences in the results among different time groups. Additionally, histological scoring was assessed using the nonparametric Mann-Whitney test. Statistical significance was defined as $P < 0.05$. Data analysis was performed using Prism 7 software (GraphPad).

3. Results

3.1. Isolation and characterization of CD56$^+$ UCSCs

Mesenchymal stem cells (MSCs) in umbilical cord are heterogeneous, resulting in lower purity that brings limited efficacy in clinic. Previous studies had demonstrated that CD56$^+$ stem cells were associated with chondrogenesis [20,21]. Therefore, we employed flow cytometry to isolate CD56$^+$ UCSCs. Initially, viable cells were selected based on being negative for Zombie as the sorting index. Subsequently, endothelial cells, red blood cells, and immune cells were eliminated by identifying negative expressions of CD31, CD235, and CD45 respectively. Furthermore, positive expressions of CD73 and CD29 were screened to identify MSCs. Finally, our target cell subpopulation was identified as CD56$^+$ UCSCs (Fig. 1A). The obtained CD56$^+$ UCSCs exhibited a long spindle shape and were cultured to the P3 generation for adipogenic, chondrogenic, and osteogenic differentiation (Fig. 1B). Flow analysis results demonstrated that cells exhibited negative expression of hematopoietic markers including CD34, CD11b, and CD45, while positive expression of MSCs markers such as CD29 and CD73 (Fig. 1C). Notably, the positive rate of CD56 was shown to be more than 90 %, indicating that the stable characteristics of these isolated CD56$^+$UCSCs were maintained during subsequent culture.

3.2. Characterization of CD56$^+$UCSC-Exos

The isolated exosomes derived from UCSCs or CD56$^+$UCSCs were characterized using NAT, TEM imaging, and WB analysis. TEM imaging revealed the characteristic cup-like morphology of UCSC-Exos and CD56$^+$UCSC-Exos exosomes, consistent with previously reported features (Fig. 1D) [23,24,39]. NAT results demonstrated that the majority of UCSC-Exos and CD56$^+$UCSC-Exos exhibited diameters ranging from 100 nm to 150 nm (Fig. 1E). Furthermore, WB analysis confirmed the identity of UCSC-Exos and CD56$^+$UCSC-Exos as exosomes by detecting exosome surface markers including TSG101, CD81, and CD63 in the isolated samples (Fig. 2F). Additionally, co-culturing experiments showed that hBMCS internalized both UCSC-Exos and CD56$^+$UCSC-Exos based on immunofluorescence results after a 12-h incubation period (Fig. 2G). Collectively, these findings provided compelling evidence supporting the classification of these nanoparticles as exosomes.

3.3. Biological evaluation of CD56$^+$UCSC-Exos

After co-culturing hBMSCs with UCSC-Exos or CD56$^+$UCSC-Exos for 14 days, alcian blue staining (Fig. 2A and E) and immunofluorescence staining (SOX9) (Fig. 2B and F) were performed to detect the expression of chondrogenic-related proteins. The results revealed that the CD56$^+$UCSC-Exos group exhibited significantly increased expression of chondrogenic-related proteins compared to the other groups in both assays. Additionally, qRT-PCR was conducted to evaluate the expression profiles of chondrogenic differentiation marker genes (SOX9, COL10, ACAN) (Fig. 2D). Remarkably, hBMSCs cultured with CD56$^+$UCSC-Exos demonstrated a specific and significant upregulation of chondrogenic genes, which mirrored the pattern observed in protein expression.

Furthermore, we assessed the chemotactic ability of CD56$^+$UCSC-Exos towards hBMSCs by quantifying migrated cells under the upper chamber. As depicted in Fig. 2C and G, the CD56$^+$UCSC-Exos group attracted a significantly higher number of cells compared to both the UCSC-Exos group and control group, indicating excellent chemotaxis effects exerted by CD56+UCSC-Exos in attracting hBMCSs.

3.4. Characterization of decellularized Wharton's jelly

In gross view, the Wharton's Jelly displayed an opalescent gel-like appearance following decellularization. Furthermore, decellularized Wharton's Jelly (DWJ) exhibited minimal cell nuclei staining when subjected to H&E or DAPI compared to the native Wharton's jelly (NWJ) (Fig. 3A). SEM revealed that the extracellular matrix (ECM) structure of DWJ exhibited increased porosity in comparison to NWJ (Fig. 3A). we conducted SR-FTIR to evaluate the levels of proteoglycan and collagen after decellularization. The results demonstrated a reduction of approximately 5.85 % in collagen content and 17.87 % in proteoglycan content within DWJ with respect to NWJ (Fig. 3A and B). The results revealed a decreasing trend in the content of proteoglycan and collagen in DWJ compared to native Wharton's Jelly, with respective contents of 1.15 ± 0.11 μg/mg and 85.94 ± 5.04 μg/mg (Fig. 3C). Additionally, the DNA content in the DWJ group exhibited a significant decrease when

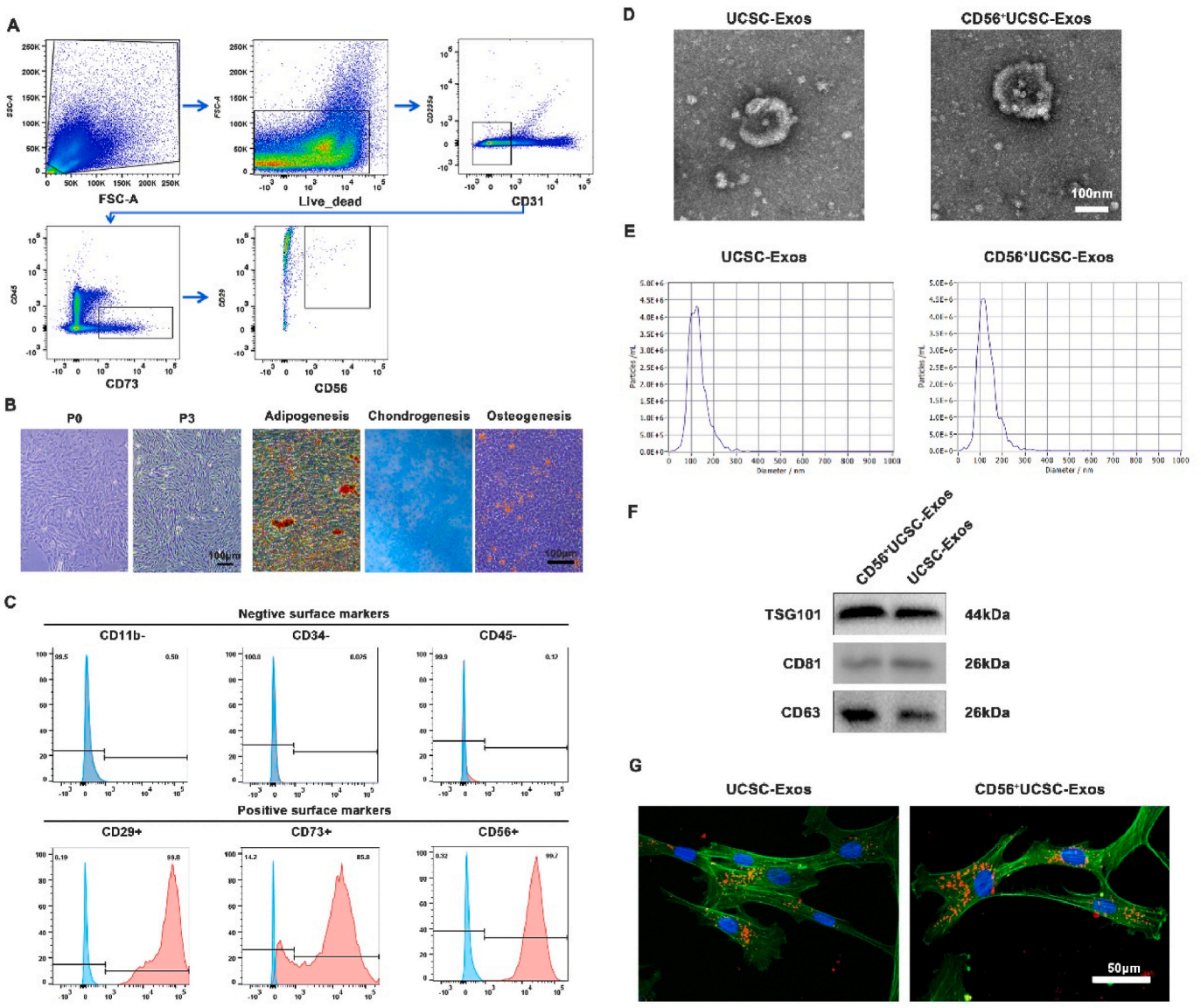

Fig. 1. Preparation and characterization of CD56$^+$UCSC-Exos. (A) Flow cytometry-based sorting of CD56$^+$UCSC population. (B) Morphological assessment and evaluation of osteogenic, lipogenic, and chondrogenic differentiation potential in CD56$^+$UCSCs. Scale bar: 100 μm. (C) Flow cytometric analysis of cellular markers expressed in CD56$^+$UCSCs. (D) Identification of exosomes using transmission electron microscopy (TEM) and (E) nanoparticle tracking analysis (NTA). Scale bar: 100 nm. (F) Western blotting analysis to determine the presence of exosomal biomarkers. (G) Immunofluorescence imaging reveals internalization of CD56$^+$UCSC-Exos or UCSC-Exos by hBMSCs. Scale bar: 50 μm.

compared to that of the native group (Fig. 3D).

3.5. *Properties and biocompatibility of DWJH/CD56$^+$Exos*

As depicted in Fig. 4A, DWJH/CD56$^+$Exos exhibited a milky fluid state. To investigate the microstructure of DWJH/CD56$^+$Exos, freeze-dried samples were subjected to SEM, revealing a loose and porous architecture (Fig. 4A). The hydrogel was loaded in the injection syringe and injected into different shapes as shown in Fig. 4B. Rheological measurements were performed to explore the mechanical properties of DWJH/CD56$^+$Exos. The injectability of the hydrogels was evaluated through shear-dependent-viscosity testing. The viscosity of the hydrogel decreased as the shear rate increased. Additionally, the elasticity and flowability properties were quantified in terms of storage modulus (G') and loss modulus (G''), where $G' > 0.1$ MPa and $G'' > 0.01$ MPa respectively (Fig. 4D). The biocompatibility of DWJH/CD56$^+$Exo was evaluated through cell viability assays. Remarkably, CCK8 results demonstrated comparable cell proliferation between the control group and the DWJH group, while the proliferation rate was significantly enhanced in the DWJH/CD56$^+$Exos group compared to other groups (Fig. 4C). Furthermore, live/dead assay results shown that no significant disparity in cell survival ratio was observed between the control group and the DWJH/CD56$^+$Exos group (Fig. 4E and F). The pro-inflammatory cytokines (TNF-a, IL-6, and IL-1β) present in the supernatant of RAW 264.7 cells were quantified to assess the proinflammatory activity of DWJH/CD56$^+$Exos. The levels of pro-inflammatory cytokines (TNF-a, IL-6, and IL-1β) secreted by RAW 264.7 cells in both the control and DWJH/CD56$^+$Exos groups exhibited no significant differences but were significantly lower compared to those observed in the LPS group (Fig. 4G). In Fig. 4H, a majority of RAW 264.7 cells displayed prominent cellular protrusions in response to LPS stimulation, while no evident cellular protrusions were observed in either the control or DWJH/CD56$^+$Exos groups.

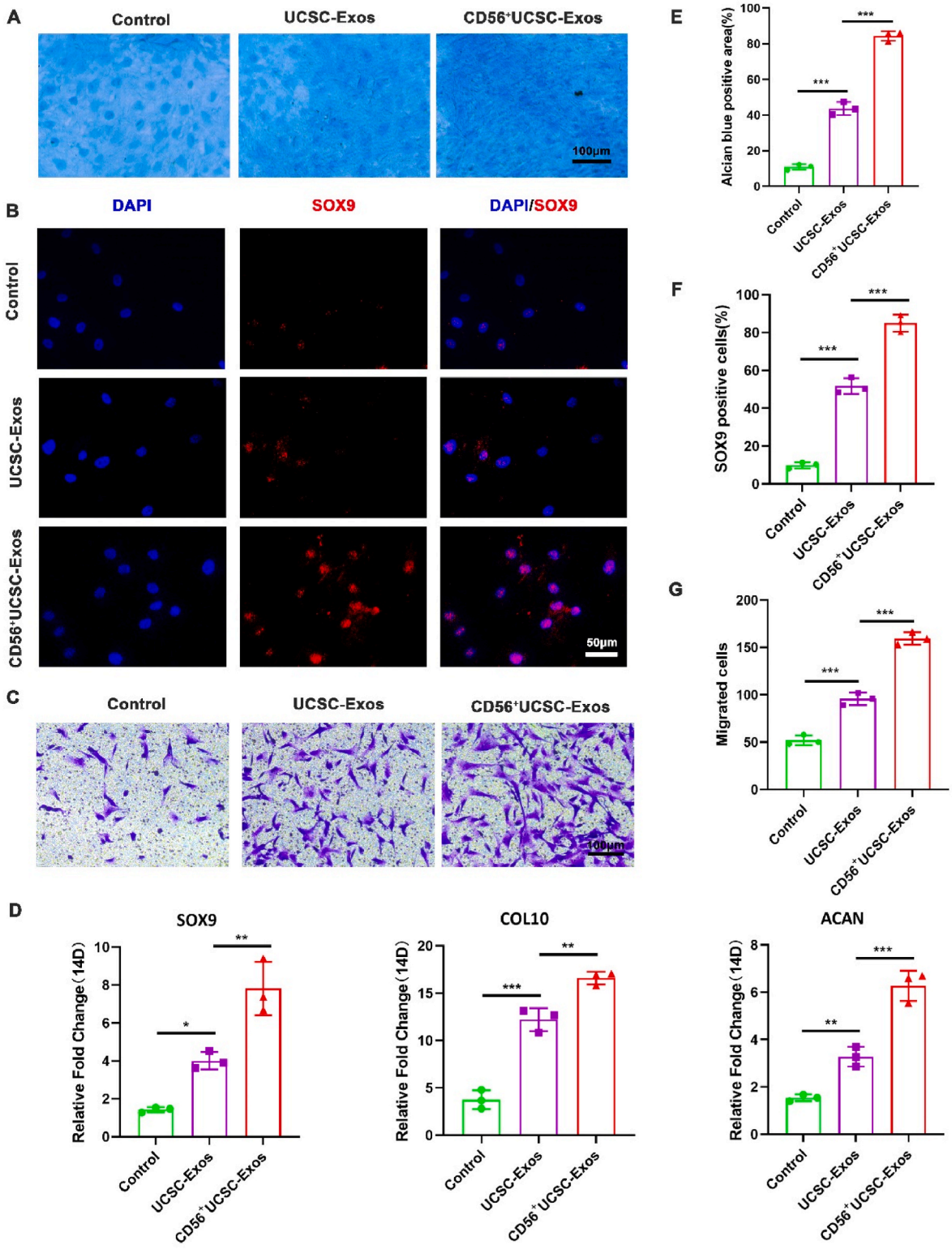

Fig. 2. Evaluation of hBMSC differentiation induced by CD56^{+}UCSC-Exos was conducted. (A) Histochemical identification using Alcian Blue staining was performed to assess chondrogenic induction of hBMSC by UCSC-Exos or CD56+UCSC-Exos. Scale bar: 100 μm. (E) Statistical analysis was carried out based on the results obtained in A. (B) Immunofluorescence staining for chondrogenic marker SOX9 was conducted and (F) quantification of positive cells was performed. (n = 3). Scale bar: 50 μm. (C) Transwell assay results demonstrated the cytocompatibility and chemotaxis differences between UCSC-Exos and CD56+UCSC-Exos (n = 3). Scale bar: 100 μm. (G) The graph illustrates disparities in cell migration between UCSC-Exos and CD56^{+}UCSC-Exos. Scale bar: 100 μm. (D) qRT-PCR analysis revealed the expression levels of key markers, including SOX9, COL10, and ANCN during hBMSC differentiation (n = 3). *$P < 0.05$, **$P < 0.01$, ***$P < 0.001$. (For interpretation of the references to colour in this figure legend, the reader is referred to the Web version of this article.)

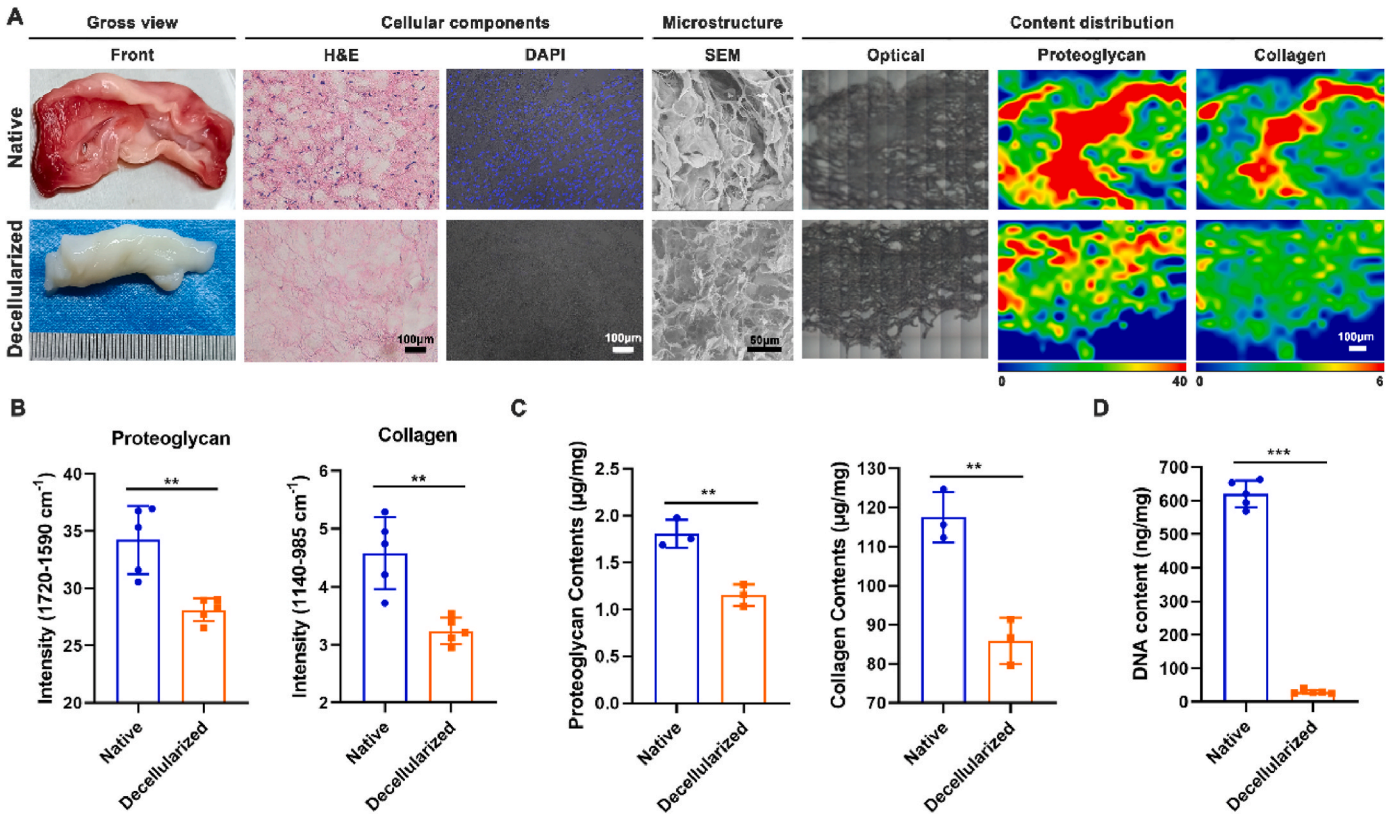

Fig. 3. Characterization of decellularized Wharton jelly. (A) Biophysical features were evaluated through macroscopic images, HE, DAPI, SEM, and SR-FTIR mappings. Scale bar: 100 μm. (B) Semi-quantitative analysis was performed to determine the collagen and proteoglycan contents in native or decellularized Wharton jelly samples. Comparative graph showing the quantitative analysis of proteoglycan (C), collagen (C) and DNA content (D) between native and decellularized Wharton jelly. $^{*}P < 0.05$, $^{**}P < 0.01$, $^{***}P < 0.001$.

3.6. Chondrogenic differentiation of hBMSCs induced by DWJH/CD56^{+}Exos

The chondrogenic differentiation potential of DWJH/CD56^{+}Exos on hBMSCs was assessed using alcian blue staining, immunofluorescence staining, and WB (SOX9, COL2, and COLX). Statistical analysis revealed consistent results between the three experiments. Notably, the DWJH/CD56^{+}Exos group exhibited significantly greater positive staining area and depth compared to other groups, while the CD56^{+}Exos group showed a significantly higher positive area than both the DWJH and control groups (Fig. 5A and D). Furthermore, immunofluorescence staining results demonstrated a consistent proportion of SOX9-positive hBMSCs across all four groups as observed in alcian blue staining (Fig. 5B and E). Compared to the control group, the other groups exhibited higher expression levels of SOX9, COL2, and COLX, while the DWJH/CD56^{+}Exos group exhibited highest expression levels (Fig. 5C and F).

3.7. Controlled release of CD56^{+}Exos from DWJH/CD56^{+}Exos

The release of CD56^{+}Exos was evaluated by immunofluorescence in vitro and in vivo imaging of small animals (IVIS Spectrum). The 3D reconstruction results in Fig. 6A showed that the red CD56^{+}Exos labeled by PKH26 were evenly distributed in DWJH and slowly released over time. Residual CD56^{+}Exos could still be detected at 21 days. The in vivo post-operated knee joint fluorescence imaging (Fig. 6B) and the results of semi-quantitative analysis (Fig. 6C) showed that the fluorescence intensity of DWJH/CD56^{+}Exos group decreased significantly slower than that of CD56^{+}Exos group, and the immunofluorescent signals of DWJH/CD56^{+}Exos group could still be detected at 21 days, while no obvious immunofluorescent signals could not be detected in CD56^{+}Exos group. The cumulative release of the PBS/CD56^{+}Exos group reached approximately 80 % by day 14, as depicted in Fig. 6D, whereas the DWJH/CD56^{+}Exos group achieved this level by day 28.

3.8. In vivo degradation of DWJH/CD56^{+}Exos

The DWJH/CD56^{+}Exos were smoothly injected into the rat dorsal region using a 26-gauge needle, resulting in the formation of a localized bolus at the injection site (Fig. 6E). After 30 min, the subcutaneous bolus underwent solidification, forming a stable subtranslucent hydrogel that retained its shape upon explanation. Over time, there was a visible reduction in volume from 30 min to 3 days and continued thinning from day 3 to day 21 (Fig. 6E). Histological analysis revealed gradual degradation of the implanted hydrogel from day 3 to day 21, accompanied by decreased infiltration of granulocytes in the central area of the hydrogel (Fig. 6F).

3.9. Evaluation of meniscus healing

Histological staining was employed to assess the healing process of torn meniscus. The H&E staining depicted in Fig. 7A revealed that the fissure in the control group remained fully trans-meniscal at 4 weeks, whereas both the DWJH/CD56^{+}Exos group and DWJH group exhibited over 50 % healing compared to the control group. The control group exhibited no evidence of self-healing within an 8-week timeframe, while significant large tears persisted and even deteriorated. Conversely, successful repair and partial healing were observed in both the DWJH/CD56^{+}Exos group and DWJH group, with smaller tear sizes respectively. The quantification of the remaining area of meniscal tears was performed (Fig. 7D), demonstrating a significantly enhanced healing effect in the DWJH/CD56^{+}Exos group compared to other experimental

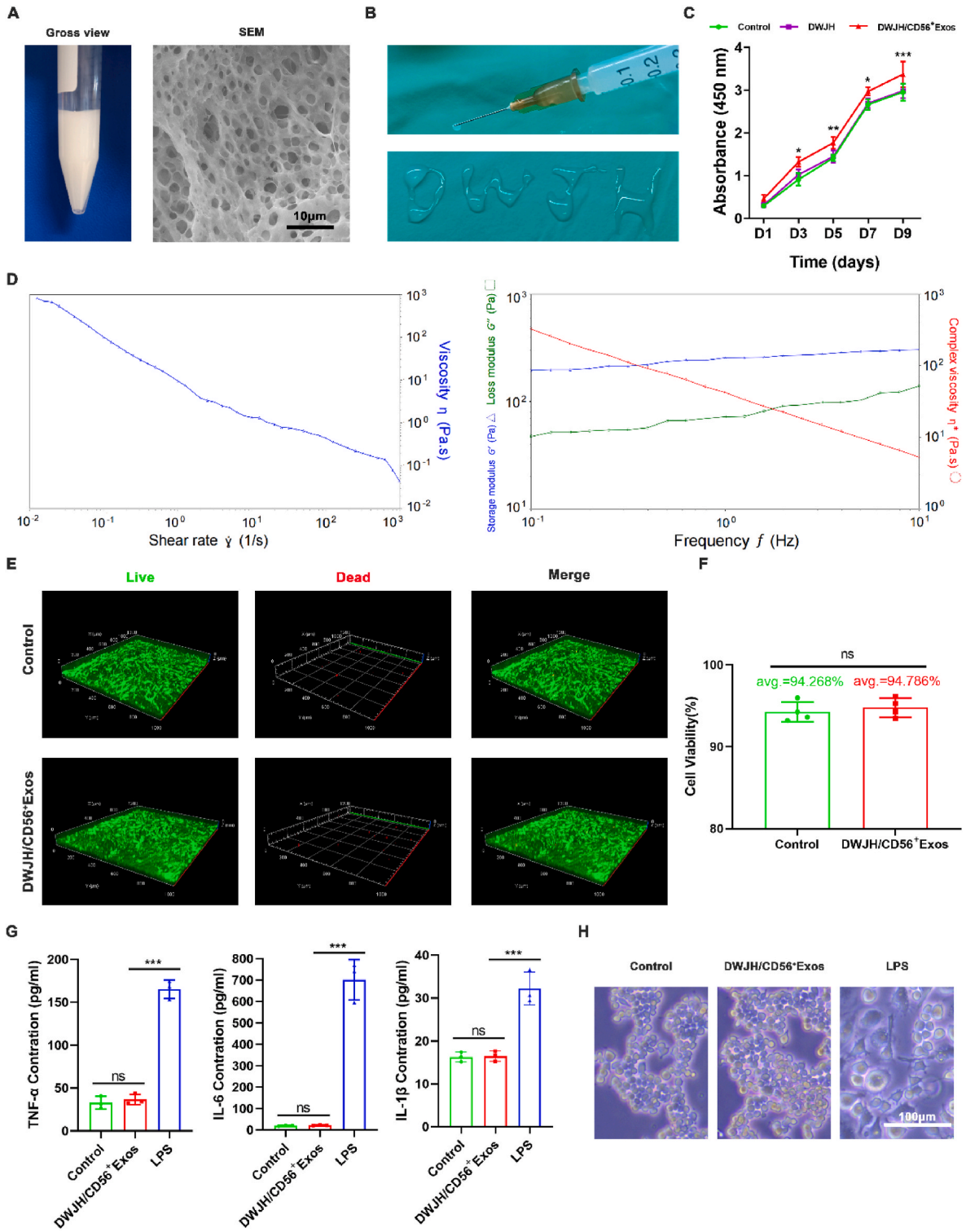

Fig. 4. Characterization and cytocompatibility of DWJH/CD56^{+}Exo were assessed using various techniques. (A) Macroscopic observation and SEM imaging of DWJH/CD56^{+}Exo. Scale bar: 10 μm. (B) The injectability of DWJH/CD56^{+}Exo. (C) Cytotoxicity analysis of DWJH/CD56^{+}Exo was assessed using the CCK-8 assay (n = 4). (D) Fluid dynamic characterization of DWJH/CD56^{+}Exo. (E) Live/dead double staining and 3D reconstruction were performed to visualize cell viability (green: live cells, red: dead cells) (n = 4). (F) Statistical analysis of the proportion of live cells in E. (G) Pro-inflammatory cytokine (TNF-α, IL-6, and IL-1β) release between control, DWJH/CD56^{+}Exo, and LPS groups after coculture for 3 days, Bar = 100 μm. (H) Representative RAW 264.7 morphology after coculture for 3 days in control, DWJH/CD56^{+}Exo, and LPS groups. $^{*}P < 0.05$, $^{**}P < 0.01$, $^{***}P < 0.001$. (For interpretation of the references to colour in this figure legend, the reader is referred to the Web version of this article.)

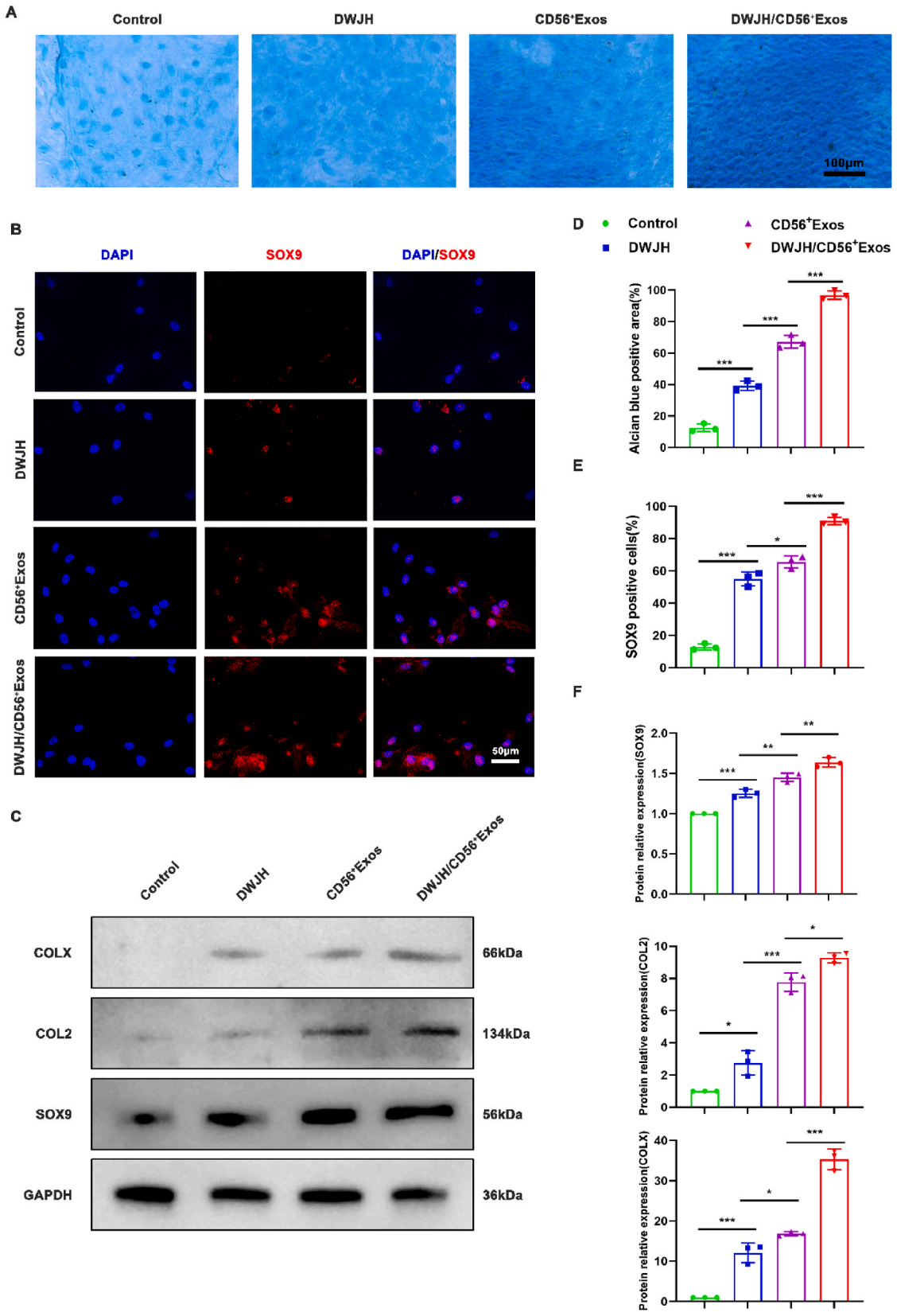

Fig. 5. Evaluation of hBMSC differentiation induced by DWJH/CD56^{+}Exos and sustained release of CD56^{+}Exos in DWJH/CD56^{+}Exos. (A) Histochemical identification using Alcian Blue staining was performed to assess chondrogenic induction of hBMSC by DWJH/CD56^{+}Exos. Scale bar: 100 μm. (E) Statistical analysis was carried out based on the results obtained in A. (B) Immunofluorescence staining for chondrogenic marker SOX9 and (F) quantification of positive cells. (n = 3). Scale bar: 50 μm. (C) Western blot of SOX9 in hBMSC treated with DWJH, CD56^{+}Exos, or DWJH/CD56^{+}Exos. (F) Quantification of SOX9, COL2, and COLX relative protein expression between different groups in control, DWJH, CD56^{+}Exos, and DWJH/CD56^{+}Exos groups. n = 3. *$P < 0.05$, **$P < 0.01$, ***$P < 0.001$. (For interpretation of the references to colour in this figure legend, the reader is referred to the Web version of this article.)

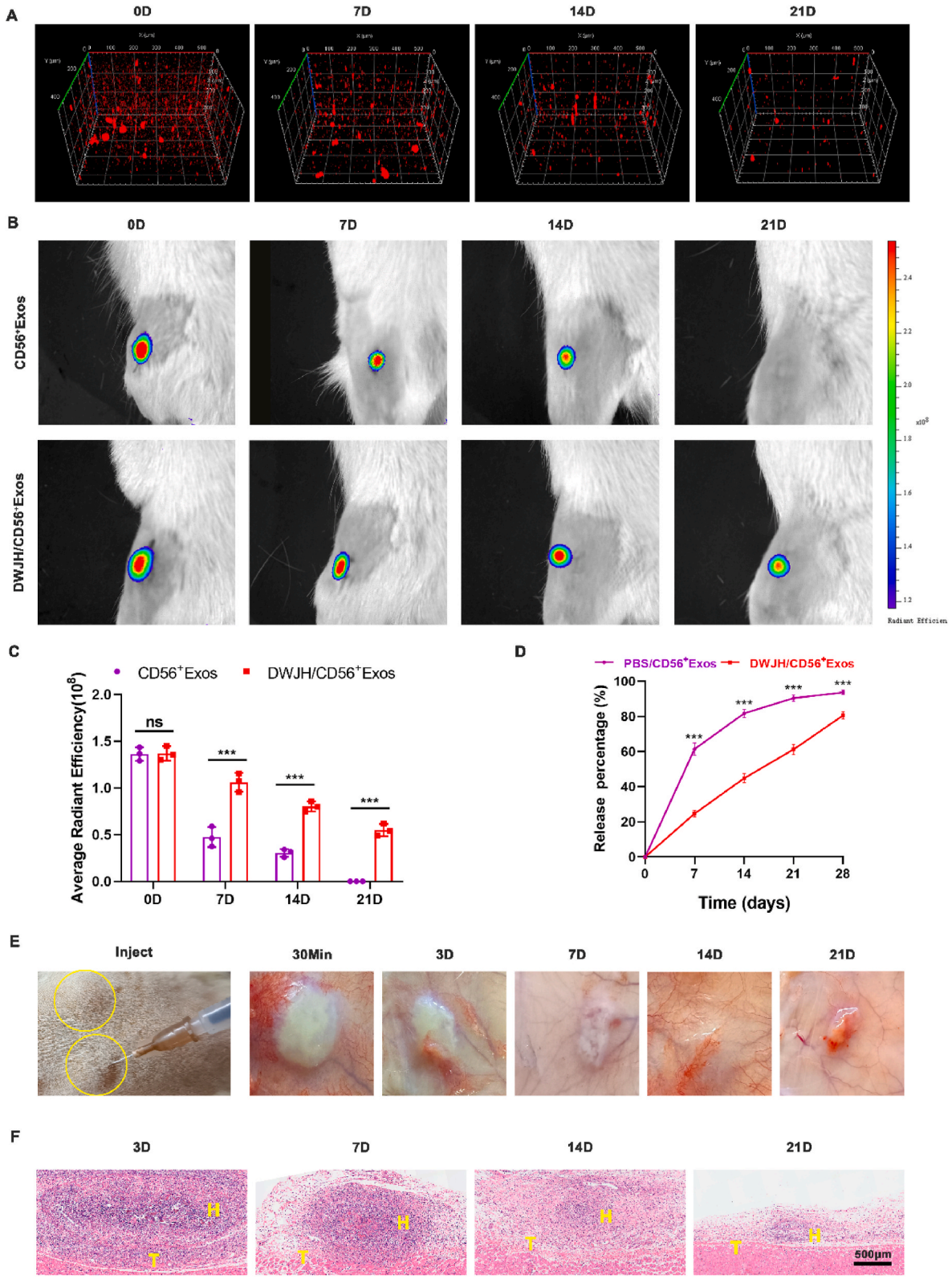

Fig. 6. Sustained release of CD56$^+$Exos and degradation of DWJH/CD56$^+$Exos. (A) In vitro fluorescence of controlled release of CD56$^+$Exos in DWJH/CD56$^+$Exos. (B) In vivo fluorescence tracking analysis demonstrated that DiR-labeled CD56$^+$Exos were delivered to the targeted area. (C) Semi-quantification analysis between the DWJH/CD56$^+$Exos group and CD56$^+$Exos group. (D) Release curves of CD56$^+$Exos from DWJH/CD56$^+$Exos at different time points. n = 5. (E) The gross view and (F) H&E staining of DWJH/CD56$^+$Exos after implantation at 30 min, 3, 7, 14, and 21 days. Yellow circles denote hydrogel bumps after injection. T: tissue; H: hydrogel. $^*P < 0.05$, $^{**}P < 0.01$, $^{***}P < 0.001$. (For interpretation of the references to colour in this figure legend, the reader is referred to the Web version of this article.)

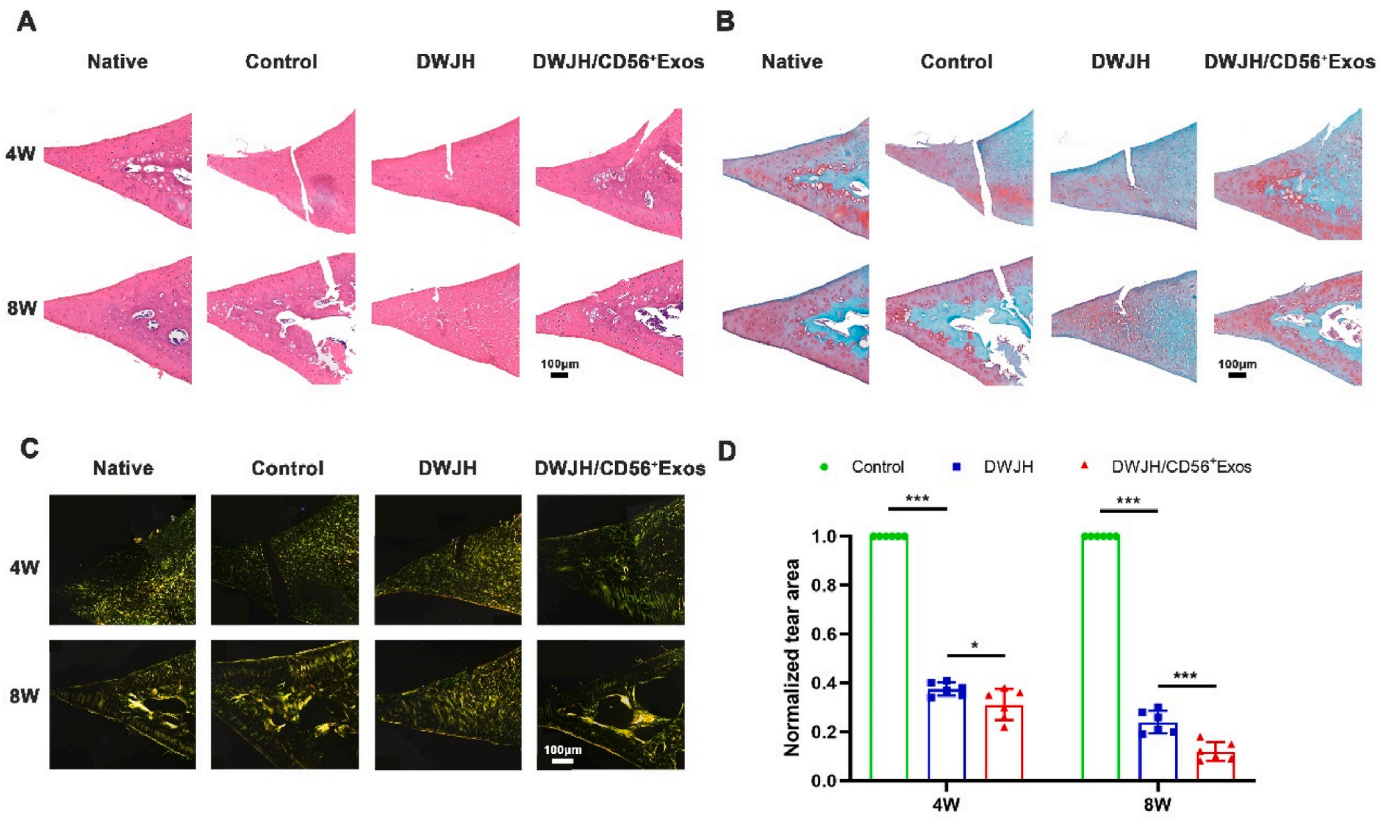

Fig. 7. Histological evaluation of meniscal tear healing. Histological analysis of native meniscus and repaired meniscal at postoperative weeks 4 and 8, including (A) hematoxylin and eosin (H&E) staining as well as (B) safranin O/fast green (SO&FG), and (C) Sirius red staining. (D) Normalized tear area after meniscus tear repair. Data are presented as mean ± SD (n = 6). Scale bar: 100 μm. (For interpretation of the references to colour in this figure legend, the reader is referred to the Web version of this article.)

groups. The meniscus proteoglycan was observed to be stained red with safranin O/fast green (SO&FG) (Fig. 7B). The extent and thickness of red area in the DWJH/CD56^{+}Exos group were less prominent than those in the native group, demonstrating significantly enhanced features when compared to both control and DWJH groups at 4 weeks and 8 weeks. Sirius red staining showed that collagen type 1 (COL1) and collagen type 3 (COL3) fibers exhibited thick and tightly arranged yellow or green fibers, respectively, while COL2 fibers formed a loose network with weak birefringence displaying various colors. As shown in Fig. 7C, more well-organized arrangement of yellow collagen resembling that of the native group was observed in the DWJH/CD56^{+}Exos group.

3.10. Histological evaluation of cartilage degeneration

Meniscal tears are commonly associated with articular cartilage injury [40]. Repairing a meniscus tear could effectively prevent degeneration of the knee joint cartilage and slow the process of osteoarthritis. To assess the progress of knee cartilage degeneration and osteoarthritis, histological staining, ICRS scores, and Mankin scores were performed on both the femoral condyle and tibial plateau of the operated side. As shown in Fig. 8A and B, there was a gradual development of osteoarthritis-like changes in the articular cartilage of both the tibial plateau and femoral condyle over time. These changes were characterized by disorganized chondrocyte arrangement, hypertrophy, and extensive exposure of subchondral bone. Compared to the control group, both DWJH group (group treated with DWJH) and DWJH/CD56^{+}Exos group (group treated with DWJH combined with CD56^{+}Exos) exhibited relatively less joint surface injury, which was shown as reduced cartilage degeneration, fewer cartilage cracks, as well as decreased exposed subchondral. However, it should be noted that these groups also experienced some degree of damage compared to normal joints over time. According to histological staining, Semi-quantitative observations along with ICRS scores and Mankin scores demonstrated that the DWJH/CD56^{+}Exos group displayed superior performance in terms of long-term preservation of cartilage followed by the DWJH group which showed significantly better results than those observed in the control group (Fig. 8C and D).

4. Discussion

The meniscal tear is a prevalent motor system injury, often resulting in cartilage degeneration and osteoarthritis of the knee joint [41,42]. Therefore, an effective treatment strategy would involve safeguarding articular cartilage against degeneration and promoting meniscus healing. In this study, we developed a novel injectable hydrogel for repairing meniscal tears called DWJH/CD56^{+}Exos, which comprised DWJH and CD56^{+}Exos. Our in vitro and in vivo findings demonstrated that DWJH/CD56^{+}Exos could continuously release CD56^{+}Exos. Furthermore, our in vitro results indicated that DWJH/CD56^{+}Exos significantly enhanced the biological activity of hBMSCs and effectively induced chondrogenic differentiation of hBMSCs. Additionally, our rat model results revealed that injectable DWJH/CD56^{+}Exos effectively promoted meniscus healing and protected knee against articular cartilage degeneration.

Numerous strategies had been developed to promote cartilage regeneration for the treatment of meniscus injuries [8,40,43]. Previous studies had demonstrated the promising potential of utilizing stem cells in addressing meniscus injury [40,42,44]. Umbilical cord mesenchymal stem cells, derived from discarded medical umbilical cords, are extensively utilized due to their non-invasive nature and remarkable activity [45,46]. However, the presence of diverse functional subpopulations within stem cells poses a significant challenge in achieving consistent,

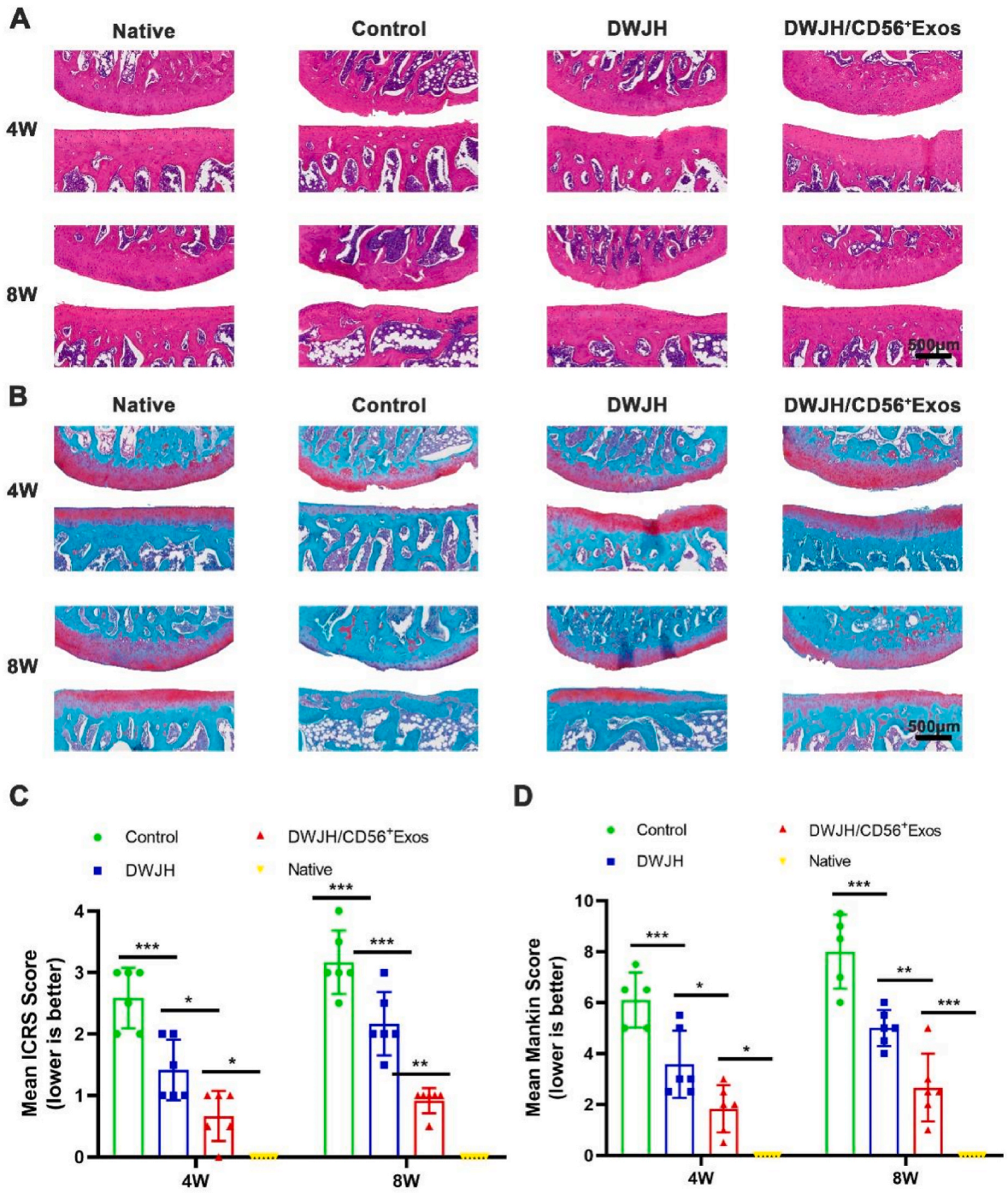

Fig. 8. Histological assessment of joint cartilage degeneration was performed using hematoxylin and eosin (H&E) (A) staining as well as safranin O/fast green (SO&FG) (B) staining on sections obtained at 4 and 8 weeks postoperatively, with the femoral condyle and tibial plateau depicted above and below, respectively. Additionally, the articular cartilage surfaces in the femoral condyle and tibial plateau were evaluated using both International Cartilage Regeneration & Joint Preservation Society (ICRS) scores(C) and Mankin scores (D) (n = 6). Scale bar: 500 μm $^{*}P < 0.05$; $^{**}P < 0.01$; $^{***}P < 0.001$. (For interpretation of the references to colour in this figure legend, the reader is referred to the Web version of this article.)

predictable, and standardized outcomes in clinical treatments [47]. Therefore, it is imperative to adopt a novel therapy that entails the identification and meticulous screening of functionally distinct subpopulations for targeted treatment. Moreover, transplantation of large numbers of cells would result in low survival rates due to local hypoxia [44,48,49]. Heterogeneity in donor's physical condition brings challenges for effective cell therapy in clinic [47]. Exosomes provide potential solutions to these challenges, as studies have demonstrated that extracellular vesicles derived from diverse stem cell sources exhibit comparable functional outcomes, rendering them a promising therapies [50].

CD56 is a glycoprotein expressed on the cell surface and is commonly associated with cells of the nervous system [51]. Previous studies have demonstrated that bone marrow mesenchymal stem cells carrying CD56 surface markers exhibit significant chondrogenic potential, as evidenced by techniques such as single-cell sequencing [20,21]. In this study, we employed flow sorting technique to screen for $CD56^{+}$ umbilical cord mesenchymal stem cells ($CD56^{+}$UCSCs). Exosomes derived from UCSCs

or CD56$^+$UCSCs were isolated and characterized to confirm their enrichment in hBMSCs. In vitro experiments, we compared the chondrogenic differentiation ability of CD56$^+$Exos and UCSC-Exos on hBMSCs based on chondrogenic differentiation-related proteins, genes, and phenotypes. The results from various assays consistently demonstrate the excellent chondrogenic differentiation induced potential of CD56$^+$Exos on hBMSCs [20].

In vivo, the rapid clearance and degradation of exosomes significantly diminished therapeutic efficacy in clinic [52]. Specifically, knee joint inflammation following meniscus tear accelerated the degradation of exosomes [53]. To address the issues, the combination of hydrogel and exosomes had garnered considerable attention [54–56]. Knee fluid showing flowing hydrogel is rich in active substances such as proteoglycan and collagen, which play a crucial role in lubricating and protecting articular cartilage [3,57]. Previous studies have demonstrated that umbilical cord-derived Wharton's jelly was abundant in proteoglycan content and could promote chondrogenic differentiation of hBMSCs [58,59]. However, Wharton's jelly might elicit an immune reaction due to its cellular components. The tissue engineering decellularization techniques could remove cellular elements and reserve the extracellular matrix (ECM) [29,60]. In this study, we successfully fabricated injectable DWJH/CD56$^+$Exos. H&E, DAPI, and DNA analysis demonstrated that the cellular components of DWJ were almost completely removed. The proteoglycan and collagen content of Semi-quantitative analysis using SR-FTIR and quantitative analysis using assay kits revealed that DWJ retained significant levels of proteoglycans and proteins. CCK8 assays and live/dead staining demonstrated excellent biocompatibility of DWJH/CD56$^+$Exos. Besides, inflammatory responses of RAW 264.7 cells revealed low proinflammatory property of DWJH/CD56$^+$Exos. The shear rate and frequency sweep analysis demonstrated that the DWJH/CD56$^+$Exos was injectable. Notably, the combination of DWJH and CD56$^+$Exos exhibited significantly enhanced chondrogenic differentiation ability compared to either DWJH or CD56$^+$Exos alone, which was observed through in vitro chondrogenic experiments. Furthermore, both in vivo and in vitro exosome release tests demonstrated that CD56$^+$Exos exhibited sustained release for over 21 days in DWJH. The in vivo degradation assay shown that the gradual degradation of the implanted DWJH/CD56$^+$Exos was accompanied with decreased infiltration of granulocytes. The results of in vivo degradation and in vitro inflammatory responses demonstrated that DWJH/CD56$^+$Exos induced low immune response, which were consistent with the published literature involving the application of decellularized tissue [29,60–62]. The prolonged release not only prevented rapid degradation of exosomes during the early inflammatory phase but also facilitated continuous promotion of cartilage repair while DWJH safeguards against cartilage degradation. Consequently, DWJH effectively delayed the degradation and release of CD56$^+$Exos.

In vivo, the results of meniscus tear healing demonstrated that DWJH/CD56$^+$Exos significantly enhanced the healing process of torn meniscus, as evidenced by histological analysis revealing improved cartilage regeneration and extracellular matrix remodeling. Moreover, histological examination and statistical analysis of the femoral condyle and tibial plateau indicated that both DWJH group and DWJH/CD56$^+$Exos group exhibited significantly less severe articular cartilage degeneration compared to the control group, suggesting a beneficial protective effect on articular cartilage following meniscus tear. Furthermore, the articular cartilage condition in the DWJH/CD56$^+$Exos group was notably superior to that in the DWJH group, which potentially attributed to a synergistic effect between the protective properties of DWJH and CD56$^+$Exos-mediated promotion of cartilage regeneration. The above findings are consistent with our previous in vitro study, which demonstrated an augmented chondrogenic potential of hBMSCs upon stimulation with DWJH/CD56+Exos. Notably, chondrocytes in the control group displayed significant reduction and pathological hypertrophy. The morphology of chondrocytes in the DWJH/CD56$^+$Exos group more closely resembled that of native tissue than other groups, which could be attributed not only to the protective effects exerted by DWJH on cartilage but also to anti-inflammatory properties conferred by CD56$^+$Exos, resulting in inhibiting progression of articular cartilage inflammation. Collectively, these findings underscored the therapeutic potential of DWJH/CD56$^+$Exos in promoting meniscal healing and protecting against articular cartilage degeneration by effectively inhibiting inflammation, thereby impeding the progression of osteoarthritis.

In this study, the group treated with CD56$^+$Exos alone was not established. The chondrogenic effect of CD56$^+$Exos had been demonstrated through in vitro cartilage differentiation experiments. The sustained release of CD56$^+$Exos in DWJH/CD56$^+$Exos was verified by both in vitro and in vivo sustained release experiments. In the absence of DWJH, CD56$^+$Exos exhibited heightened susceptibility to degradation, while articular cartilage lacking DWJH protection accelerated degeneration, thereby further expediting the degradation of CD56$^+$Exos. Moreover, a reduced sample size was employed in consideration of ethical concerns pertaining to animal welfare. Although in vivo immunogenicity test was not conducted in this study, previous studies had demonstrated that acellular tissue with complete removal of cell components exhibits minimal immunogenicity. Additionally, the complete removal of cell components of DWJ was confirmed with H&E, and DAPI staining. Additionally, the complete removal of cell components of DWJ was confirmed with H&E staining, DAPI staining, and DNA content quantification. Further CCK8 and live/dead staining supported the favorable biocompatibility of DWJH/CD56$^+$Exos.

However, it should be acknowledged that there was limitation in this study. such as the mechanism of DWJH/CD56$^+$Exos in promoting meniscus healing and protecting against articular cartilage degeneration. Future investigations need to elucidate the specific cellular signaling pathways induced by DWJH/CD56$^+$Exos. Despite these limitations, our injectable DWJH/CD56$^+$Exos demonstrated promising potential for clinical applications in the treatment of meniscus tears.

5. Conclusion

We developed an injectable hydrogel named DWJH/CD56$^+$Exos for meniscus tear. It was extensively investigated through in vivo and in vitro experiments that the optimized hydrogel demonstrated remarkable potential for clinical applications in the treatment of meniscus tear by promoting torn meniscus healing, safeguarding articular cartilage, and inhibiting secondary cartilage degeneration. The DWJH/CD56$^+$Exos might serve as a promising potential therapy for clinical meniscus tear.

Funding statement

This study was supported by the Key Program of the National Natural Science Foundation of China. (NO.82230085 and NO.82272572), the Science and Technology Major Project of Changsha. (NO.kh2003015), the Research and Development Program in Key Areas of Hunan Province. (NO.2020SK2077).

CRediT authorship contribution statement

Simiao Kang: Writing – original draft, Visualization, Software, Methodology, Investigation, Data curation, Conceptualization. **Xin Shi:** Writing – original draft, Software, Methodology, Investigation, Data curation, Conceptualization. **Yong Chen:** Software, Methodology. **Lin Zhang:** Formal analysis, Data curation. **Quanbo Liu:** Formal analysis, Data curation. **Ziyang Lin:** Formal analysis, Data curation. **Hongbin Lu:** Writing – review & editing, Resources, Project administration, Funding acquisition, Conceptualization. **Haile Pan:** Writing – review & editing, Supervision, Project administration, Conceptualization.

Declaration of competing interest

The authors declare that they have no known competing financial

interests or personal relationships that could have appeared to influence the work reported in this paper.

Data availability

No data was used for the research described in the article.

Acknowledgement

We thank the staff from BL01B beamline of the National Facility for Protein Science in Shanghai (NFPS) at Shanghai Synchrotron Radiation Facility, for assistance during data collection.

References

[1] K. Messner, J. Gao, The menisci of the knee joint. Anatomical and functional characteristics, and a rationale for clinical treatment, J. Anat. 193 (Pt 2) (1998) 161–178.
[2] H. Kwon, W.E. Brown, C.A. Lee, et al., Surgical and tissue engineering strategies for articular cartilage and meniscus repair, Nat. Rev. Rheumatol. 15 (9) (2019) 550–570.
[3] K.I. Lee, R. Gamini, M. Olmer, et al., Mohawk is a transcription factor that promotes meniscus cell phenotype and tissue repair and reduces osteoarthritis severity, Sci. Transl. Med. 12 (567) (2020).
[4] M. Englund, F.W. Roemer, D. Hayashi, M.D. Crema, A. Guermazi, Meniscus pathology, osteoarthritis and the treatment controversy, Nat. Rev. Rheumatol. 8 (7) (2012) 412–419.
[5] S. Hashimoto, T. Ichinose, T. Ohsawa, N. Koibuchi, H. Chikuda, Extracorporeal shockwave therapy accelerates the healing of a meniscal tear in the avascular region in a rat model, Am. J. Sports Med. 47 (12) (2019) 2937–2944.
[6] S. Tarafder, J. Gulko, D. Kim, et al., Effect of dose and release rate of CTGF and TGFβ3 on avascular meniscus healing, J. Orthop. Res. 37 (7) (2019) 1555–1562.
[7] B.B. Rothrauff, H. Sasaki, S. Kihara, et al., Point-of-Care procedure for enhancement of meniscal healing in a goat model utilizing infrapatellar fat pad-derived stromal vascular fraction cells seeded in photocrosslinkable hydrogel, Am. J. Sports Med. 47 (14) (2019) 3396–3405.
[8] A. Bandyopadhyay, B. Ghibhela, B.B. Mandal, Current advances in engineering meniscal tissues: insights into 3D printing, injectable hydrogels and physical stimulation based strategies, Biofabrication 16 (2) (2024).
[9] K. Ciemniewska-Gorzela, P. Bąkowski, J. Naczk, R. Jakob, T. Piontek, Complex meniscus tears treated with collagen matrix wrapping and bone marrow blood injection: clinical effectiveness and survivorship after a minimum of 5 Years' follow-up, Cartilage 13 (1_suppl) (2021) 228S–238S.
[10] R. Resmi, J. Parvathy, A. John, R. Joseph, Injectable self-crosslinking hydrogels for meniscal repair: a study with oxidized alginate and gelatin, Carbohydr. Polym. 234 (2020) 115902.
[11] H. Sasaki, B.B. Rothrauff, P.G. Alexander, et al., In vitro repair of meniscal radial tear with hydrogels seeded with adipose stem cells and TGF-β3, Am. J. Sports Med. 46 (10) (2018) 2402–2413.
[12] F.-X. Zhang, Y. Dou, B. Zhang, et al., Skeletal stem cell-derived exosomes promote meniscal tear healing and ameliorate secondary osteoarthritis, Am. J. Sports Med. 52 (10) (2024) 2512–2523.
[13] Y. Wang, H. Xu, J. Wang, H. Yi, Y. Song, Extracellular vesicles in the pathogenesis, treatment, and diagnosis of spinal cord injury: a mini-review, Curr. Stem Cell Res. Ther. 17 (4) (2022) 317–327.
[14] L. Pang, H. Jin, Z. Lu, et al., Treatment with mesenchymal stem cell-derived nanovesicle-containing gelatin methacryloyl hydrogels alleviates osteoarthritis by modulating chondrogenesis and macrophage polarization, Adv Healthc Mater 12 (17) (2023) e2300315.
[15] Y. Bie, Q. Chen, J. Xu, et al., Human umbilical-cord-derived mesenchymal stem cells in combination with rapamycin reduce cartilage degradation via inhibition of the AKT/mTOR signaling pathway, Immunopharmacol. Immunotoxicol. 45 (5) (2023) 549–557.
[16] H. Zhou, X. Shen, C. Yan, et al., Extracellular vesicles derived from human umbilical cord mesenchymal stem cells alleviate osteoarthritis of the knee in mice model by interacting with METTL3 to reduce m6A of NLRP3 in macrophage, Stem Cell Res. Ther. 13 (1) (2022) 322.
[17] J. Galipeau, L. Sensébé, Mesenchymal stromal cells: clinical challenges and therapeutic opportunities, Cell Stem Cell 22 (6) (2018) 824–833.
[18] O. Levy, R. Kuai, E.M.J. Siren, et al., Shattering barriers toward clinically meaningful MSC therapies, Sci. Adv. 6 (30) (2020) eaba6884.
[19] Q.-F. Han, W.-J. Li, K.-S. Hu, et al., Exosome biogenesis: machinery, regulation, and therapeutic implications in cancer, Mol. Cancer 21 (1) (2022) 207.
[20] V.L. Battula, S. Treml, P.M. Bareiss, et al., Isolation of functionally distinct mesenchymal stem cell subsets using antibodies against CD56, CD271, and mesenchymal stem cell antigen-1, Haematologica 94 (2) (2009) 173–184.
[21] Z. Wang, X. Li, J. Yang, et al., Single-cell RNA sequencing deconvolutes the in vivo heterogeneity of human bone marrow-derived mesenchymal stem cells, Int. J. Biol. Sci. 17 (15) (2021) 4192–4206.
[22] R. Kalluri, V.S. LeBleu, The biology, function, and biomedical applications of exosomes, Science 367 (6478) (2020).
[23] X. Shi, Y. Li, S. Kang, et al., Dual-functional gallium/chitosan/silk/umbilical cord mesenchymal stem cell exosome sponge scaffold for diabetic wound by angiogenesis and antibacteria, Int. J. Biol. Macromol. 274 (Pt 2) (2024) 133420.
[24] Y. Sun, Q. Liu, Y. Qin, et al., Exosomes derived from CD271+CD56+ bone marrow mesenchymal stem cell subpopoulation identified by single-cell RNA sequencing promote axon regeneration after spinal cord injury, Theranostics 14 (2) (2024) 510–527.
[25] L. Penolazzi, A. Chierici, M.P. Notarangelo, et al., Wharton's jelly-derived multifunctional hydrogels: new tools to promote intervertebral disc regeneration in vitro and ex vivo, J. Biomed. Mater. Res. 112 (7) (2024) 973–987.
[26] L. Penolazzi, M. Pozzobon, L.S. Bergamin, et al., Extracellular matrix from decellularized Wharton's jelly improves the behavior of cells from degenerated intervertebral disc, Front. Bioeng. Biotechnol. 8 (2020) 262.
[27] N. Saulnier, E. Viguier, E. Perrier-Groult, et al., Intra-articular administration of xenogeneic neonatal Mesenchymal Stromal Cells early after meniscal injury down-regulates metalloproteinase gene expression in synovium and prevents cartilage degradation in a rabbit model of osteoarthritis, Osteoarthritis Cartilage 23 (1) (2015) 122–133.
[28] Q. Chen, Y. Jin, T. Chen, et al., Injectable nanocomposite hydrogels with enhanced lubrication and antioxidant properties for the treatment of osteoarthritis, Mater Today Bio 25 (2024) 100993.
[29] Y. Tang, C. Chen, F. Liu, et al., Structure and ingredient-based biomimetic scaffolds combining with autologous bone marrow-derived mesenchymal stem cell sheets for bone-tendon healing, Biomaterials 241 (2020) 119837.
[30] X.-J. Zhou, H.-C. Zhu, J.-J. Zhong, et al., New status of the infrared beamlines at SSRF, Nucl. Sci. Tech. 30 (12) (2019) 182.
[31] Y. Zhou, C. Chen, Z. Guo, et al., SR-FTIR as a tool for quantitative mapping of the content and distribution of extracellular matrix in decellularized book-shape bioscaffolds, BMC Musculoskelet Disord 19 (1) (2018) 220.
[32] B.B. Rothrauff, K. Shimomura, R. Gottardi, P.G. Alexander, R.S. Tuan, Anatomical region-dependent enhancement of 3-dimensional chondrogenic differentiation of human mesenchymal stem cells by soluble meniscus extracellular matrix, Acta Biomater. 49 (2017) 140–151.
[33] G. Yang, B.B. Rothrauff, H. Lin, et al., Enhancement of tenogenic differentiation of human adipose stem cells by tendon-derived extracellular matrix, Biomaterials 34 (37) (2013) 9295–9306.
[34] D.A. Young, D.O. Ibrahim, D. Hu, K.L. Christman, Injectable hydrogel scaffold from decellularized human lipoaspirate, Acta Biomater. 7 (3) (2011) 1040–1049.
[35] S. Desai, M. Dooner, J. Newberry, et al., Stable human cartilage progenitor cell line stimulates healing of meniscal tears and attenuates post-traumatic osteoarthritis, Front. Bioeng. Biotechnol. 10 (2022) 970235.
[36] Y. Kawanishi, T. Nakasa, T. Shoji, et al., Intra-articular injection of synthetic microRNA-210 accelerates avascular meniscal healing in rat medial meniscal injured model, Arthritis Res. Ther. 16 (6) (2014) 488.
[37] D. Jiang, L.-H. Zhao, M. Tian, J.-Y. Zhang, J.-K. Yu, Meniscus transplantation using treated xenogeneic meniscal tissue: viability and chondroprotection study in rabbits, Arthroscopy 28 (8) (2012) 1147–1159.
[38] H.J. Mankin, H. Dorfman, L. Lippiello, A. Zarins, Biochemical and metabolic abnormalities in articular cartilage from osteo-arthritic human hips. II. Correlation of morphology with biochemical and metabolic data, J Bone Joint Surg Am. 53 (3) (1971) 523–537.
[39] J.J. Lai, Z.L. Chau, S.-Y. Chen, et al., Exosome processing and characterization approaches for research and technology development, Adv. Sci. 9 (15) (2022) e2103222.
[40] X. Pan, R. Li, W. Li, et al., Silk fibroin hydrogel adhesive enables sealed-tight reconstruction of meniscus tears, Nat. Commun. 15 (1) (2024) 2651.
[41] K.I. Lee, S. Choi, T. Matsuzaki, et al., FOXO1 and FOXO3 transcription factors have unique functions in meniscus development and homeostasis during aging and osteoarthritis, Proc Natl Acad Sci U S A. 117 (6) (2020) 3135–3143.
[42] J. Sun, Y.T. Chan, K.W.K. Ho, et al., "Slow walk" mimetic tensile loading maintains human meniscus tissue resident progenitor cells homeostasis in photocrosslinked gelatin hydrogel, Bioact. Mater. 25 (2023) 256–272.
[43] S. Dadoo, L.E. Keeling, I.D. Engler, et al., Higher odds of meniscectomy compared with meniscus repair in a young patient population with increased neighbourhood disadvantage, Br. J. Sports Med. 58 (12) (2024) 649–654.
[44] S. Oyama, T. Kanamoto, K. Ebina, et al., Cyclic compressive loading induces a mature meniscal cell phenotype in mesenchymal stem cells with an atelocollagen-based scaffold, Front. Bioeng. Biotechnol. 12 (2024) 1394093.
[45] L. Li, J. Li, H. Guan, et al., Human umbilical cord mesenchymal stem cells in diabetes mellitus and its complications: applications and research advances, Int. J. Med. Sci. 20 (11) (2023) 1492–1507.
[46] A. Naji, M. Eitoku, B. Favier, et al., Biological functions of mesenchymal stem cells and clinical implications, Cell. Mol. Life Sci. 76 (17) (2019) 3323–3348.
[47] Z. Wang, C. Chai, R. Wang, et al., Single-cell transcriptome atlas of human mesenchymal stem cells exploring cellular heterogeneity, Clin. Transl. Med. 11 (12) (2021) e650.
[48] G. Ding, J. Du, X. Hu, Y. Ao, Mesenchymal stem cells from different sources in meniscus repair and regeneration, Front. Bioeng. Biotechnol. 10 (2022) 796367.
[49] X. Li, D. Li, J. Li, et al., Preclinical studies and clinical trials on cell-based treatments for meniscus regeneration, Tissue Eng Part B Rev 29 (6) (2023) 634–670.
[50] Andaloussi S. El, I. Mäger, X.O. Breakefield, M.J.A. Wood, Extracellular vesicles: biology and emerging therapeutic opportunities, Nat. Rev. Drug Discov. 12 (5) (2013) 347–357.
[51] C.K. Frese, M. Mikhaylova, R. Stucchi, et al., Quantitative map of proteome dynamics during neuronal differentiation, Cell Rep. 18 (6) (2017) 1527–1542.

[52] L. Barile, G. Vassalli, Exosomes: therapy delivery tools and biomarkers of diseases, Pharmacol. Ther. 174 (2017) 63–78.
[53] Y. Xue, N. Riva, L. Zhao, et al., Recent advances of exosomes in soft tissue injuries in sports medicine: a critical review on biological and biomaterial applications, J Control Release 364 (2023).
[54] M.-H. Fan, J.-K. Pi, C.-Y. Zou, et al., Hydrogel-exosome system in tissue engineering: a promising therapeutic strategy, Bioact. Mater. 38 (2024).
[55] Y. Kang, J. Xu, La Meng, et al., 3D bioprinting of dECM/Gel/QCS/nHAp hybrid scaffolds laden with mesenchymal stem cell-derived exosomes to improve angiogenesis and osteogenesis, Biofabrication 15 (2) (2023).
[56] B. Liu, O.A. Alimi, Y. Wang, et al., Differentiated mesenchymal stem cells-derived exosomes immobilized in decellularized sciatic nerve hydrogels for peripheral nerve repair, J Control Release 368 (2024) 24–41.
[57] S. Bansal, E.R. Floyd, M. A Kowalski, et al., Meniscal repair: the current state and recent advances in augmentation, J. Orthop. Res. 39 (7) (2021) 1368–1382.
[58] L. Penolazzi, A. Chierici, M.P. Notarangelo, et al., Wharton's jelly-derived multifunctional hydrogels: new tools to promote intervertebral disc regeneration in vitro and ex vivo, J. Biomed. Mater. Res. 112 (7) (2024) 973–987.
[59] L. Wang, Y. Liu, Z. Lin, et al., Durable immunomodulatory hierarchical patch for rotator cuff repairing, Bioact. Mater. 37 (2024) 477–492.
[60] T. Zhang, X. Shi, M. Li, J. Hu, H. Lu, Optimized allogenic decellularized meniscal scaffold modified by collagen affinity stromal cell-derived factor SDF1α for meniscal regeneration: a 6- and 12-week animal study in a rabbit model, Am. J. Sports Med. 52 (1) (2024) 124–139.
[61] L. Lian, M. Xie, Z. Luo, et al., Rapid volumetric bioprinting of decellularized extracellular matrix bioinks, Adv Mater 36 (34) (2024) e2304846.
[62] X. Shi, L. Jiang, X. Zhao, et al., Adipose-derived stromal cell-sheets sandwiched, book-shaped acellular dermal matrix capable of sustained release of basic fibroblast growth factor promote diabetic wound healing, Front. Cell Dev. Biol. 9 (2021) 646967.